

# Experimental comparison of nonlinear motion control methods for a variable stiffness actuator\*

P. Erler<sup>1</sup>, P. Beckerle<sup>1,2</sup>, B. Strah<sup>1,2</sup> and S. Rinderknecht<sup>1</sup>

**Abstract**—Variable compliant actuators play a key role in the development of efficient biomechatronic systems since energy can be stored in the compliant element thus leading to consumption reduction. In this paper, experimental results comparing passivity-based control (PBC) and feedback linearization (FL) for motion control of an actuator with variable torsional stiffness (VTS) aiming at applications like prosthetic knee joints are presented. The concept of VTS and the experimental setup are described and a mathematical model of the latter one is derived. Based on this, a control architecture consisting of an extended Kalman filter (EKF) to estimate the velocities, a friction compensation as well as the mentioned controller types is developed. Both control methods are analyzed in terms of accuracy, dynamics and their control torque. FL and PBC lead to a stable control with high performance whereas the robustness is low by reason of the model-based control design. FL is superior to the PBC in terms of accuracy and control torque, which is mainly due to the high sensitivity of PBC regarding the discrete position signals. In addition, it is shown that FL can be applied for stable operation near the second natural frequency for different stiffness values.

## I. INTRODUCTION

With closer interaction of humans and robots, safety aspects have received increased priority in robotic design in the the last decades. A widely adopted approach to ensure safety are compliant actuation concepts including serial elasticity. Those can further be used for energy storage and thus optimize drive train efficiency and decrease power consumption [1]. Adjusting the stiffness can provide additional advantages by matching the natural frequency of the compliant drive train to the frequency of the desired trajectory [2]–[4]. First compliant actuators with variable stiffness like the Series Elastic Actuator (SEA) [2], [5] or the Mechanical Impedance Adjuster (MIA) [6] were introduced in the 1990s. The variety of concepts that emerged since then can be categorized in four groups of fundamental stiffness variation principles according to [1]: Equilibrium-controlled, antagonistic-controlled, structure-controlled and mechanically controlled stiffness. In a more recent review [7], the latter three are categorized as actuators with adaptable compliance properties in contrast to such with fixed compliance like the equilibrium-controlled SEA. The latter ones change the equilibrium position of a spring [8]. In antagonistic-controlled concepts, actuators are coupled antagonistically via springs to reach adaptable stiffness as

in AMASC [9]. Many concepts proposed recently, belong to structure-controlled and mechanically controlled categories. Structure-controlled ones change stiffness by a modification of the physical structure of an elastic element as in MIA, while mechanically controlled approaches like MAC-CEPA [10] adjust the system stiffness by pretension.

The authors' approach is based on variable torsional stiffness (VTS) and aims at an application in biomechanically inspired robotic joints as in lower limb prostheses [11]. As the torsional joint stiffness is adjusted by varying the length of an elastic element, it belongs to the structure-controlled variable compliant actuators. The concept described in [11] enables compact actuators with a large stiffness bandwidth and customizable dynamic characteristics.

A crucial point for practical application of such a concept is the selection of a suitable control structure. For the purpose of motion control, an actuator based on VTS represents a flexible-joint robot (FJR). A large quantity of different controllers for such systems have been investigated in the last three decades. Among those, proportional-derivative (PD) control with its simple structure is a widely adopted approach [12]. Such methods provide high robustness but show limitations in control performance. Higher performance can be achieved with model-based controllers, like singular perturbation (SP) techniques [13], passivity-based control (PBC) [14] and feedback linearization (FL) [15]. PBC is used in combination with joint torque sensors for position control of a lightweight robot as in [14], [16] and FL is applied to a robot with variable-joint stiffness (VSA) by adapting the control law in [17]. In [18], a simulative evaluation of the VTS actuator driving a pendulum using FL could show that FL is a suitable control law to exploit the advantages of the VTS concept.

In this paper, FL and PBC are experimentally compared for motion control of a pendulum driven by a prototypic VTS actuator. After a brief repetition of the VTS concept and an introduction of the test rig, a model of the drive train mechanics and an analysis of its dynamics are given in Section II. Based on the analysis, Section III illustrates the control architecture including FL and PBC as control laws as well as the implementation of a friction compensation and an extended Kalman filter estimating velocities to achieve full state feedback. Experimental results comparing FL and PBC during specific motion tasks are presented in Section IV. Section V covers the conclusions and an outlook.

\*This work was funded by Forum for Interdisciplinary Research of Technische Universität Darmstadt.

<sup>1</sup> Institute for Mechatronic Systems, Department of Mechanical Engineering, Technische Universität Darmstadt, lastname@ims.tu-darmstadt.de

<sup>2</sup> Member, IEEE

## II. DYNAMICS MODELING AND ANALYSIS

The concept and modules of the VTS actuator are given in Figure 1 as well as the control architecture of the algorithms described in Section III. Actuator 1 applies a torque  $\tau_i$  to the torsional elastic element and drives a pendulum. The adjustment of the torsional drive train stiffness  $k_{vts}(y)$  is implemented by varying the effective length  $y$  of the elastic element via the location of a counter bearing using actuator 2. Due to the separation of the actuators driving the joint and setting stiffness, this adjustment is conducted independently from the position control in idle state and during operation. Since the focus of this paper is on the motion control, the modeling of the stiffness control path is not considered. In this section, the experimental setup will be described and the transfer behaviour of the compliant drive train is modeled and analyzed.

### A. Experimental Setup

Figure 2 shows the experimental VTS setup and names the mechanical components. Actuator 1 is a brushed DC motor with a rated power of  $P_{act} = 200 W$ , a rated torque of  $\tau_{act} = 0.6 Nm$  and a rated speed of  $n_{act} = 3000 rpm$ . A gearbox with a ratio of  $i_g = 80$  is attached to the drive. For the connection to the elastic element a bellows coupling that compensates for deflection is chosen. Within the aluminium tube, an elastic element and a counter bearing are located. Note that the elastic element is fixed to the coupling and can freely rotate on the output side, hence the torque is transmitted between counter bearing and pendulum through the aluminium tube. The stiffness adjustment mechanism is deinstalled for the experiments shown here and thus, the active elastic length is varied manually. To measure the drive side position  $q_i$  and pendulum position  $q_o$  a 360 cpr incremental encoder and an 1024 cpr incremental encoder is used respectively.

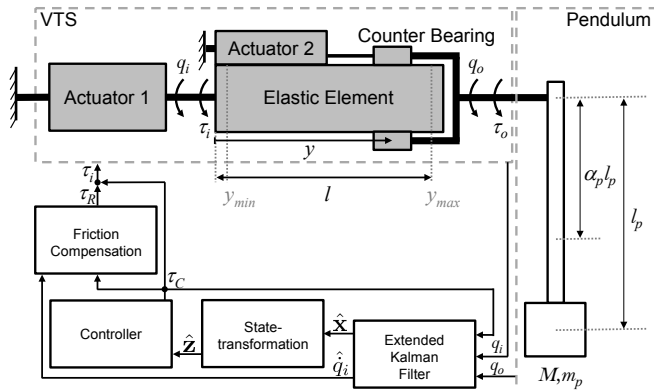


Fig. 1. VTS concept and block diagram of control.

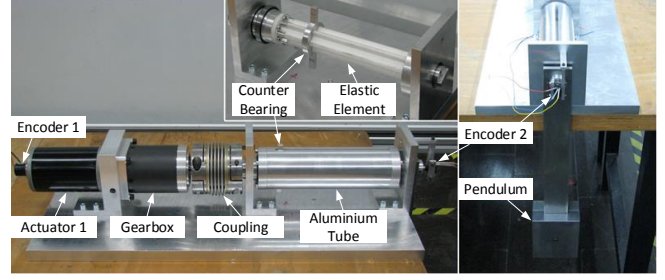


Fig. 2. Photos of the experimental VTS setup: Side view of the VTS actuator (Left), inside of the aluminium tube (upper middle) and the pendulum (right)



Fig. 3. Mechanical model of the VTS drive train.

### B. Model of Actuator Mechanics

The torsional elasticity is modeled by

$$\tau_t = k_{vts}(y) (q_o - q_i) = \frac{\Gamma I_t(y)}{y} (q_o - q_i). \quad (1)$$

In this, the difference of the output position  $q_o$  and the input position  $q_i$  is induced by the torsional torque  $\tau_t$  of the elastic element, which is equal to  $-\tau_o$  in Figure 1. The torsional stiffness  $k_{vts}(y)$  of the elastic element is described using the modulus of elasticity in shear  $\Gamma$  of the material as well as the active length  $y$  and the torsional moment of inertia  $I_t(y)$  of the elastic element. The experimental setup shown in Figure 2 can be modeled as two elastically coupled inertias with a gravitational torque  $G$  taking effect on the pendulum side. Figure 3 shows the resulting mechanical model. Regarding the link side, the moment of inertia of the pendulum is  $M = m_p (\alpha_p l_p)^2 + I_p$ . The actuator inertia  $I_m$ , gear inertia  $I_g$  and coupling inertia  $I_c$  can be summarized to the reduced inertia  $J = i_g^2 I_m + I_g + I_c$  according to [19]. The input torque  $\tau_i$  equals the transformed drive torque  $i_g \tau_{act}$  at the gear output.  $G$  accounts for gravity torques and is given by  $G = m_p g \alpha_p l_p \sin(q_o)$ . Applying the Euler-Lagrange equations leads to the following equations of motion

$$M \ddot{q}_o + G(q_o) + k_{vts} (q_o - q_i) = 0, \quad (2)$$

$$J \ddot{q}_i - k_{vts} (q_o - q_i) = \tau_i. \quad (3)$$

The mechanical parameters of the setup are given in Table I.

### C. Model Analysis

In [18], a model analysis focusing on drive train power consumption is presented. Three areas of minimum consumption of the power  $P_{m,i} = \tau_i \dot{q}_i$  are located on a plane spanned by vectors of varying stiffness  $k_{vts}$  and motion frequency  $f_s$ . Two of those minima show high dependency regarding the variation of stiffness and can be used to adapt the

system dynamics to the desired motion. Motivated by these results, the transfer behaviors of  $\frac{q_o}{\tau_i}$  and  $\frac{q_o}{q_i}$  are investigated using Bode diagrams to get insights into the requirements for control design. Choosing  $q_o = 0^\circ$  as operating point the transfer functions of the linearized model (2)-(3) are given by

$$\frac{q_o}{\tau_i} = \frac{k_{vts}}{a_4 s^4 + a_2 s^2 + a_0} \quad (4)$$

with

$$\begin{aligned} a_4 &= JM \\ a_2 &= (J + M)k_{vts} + Jm_p l_p \alpha_p g \\ a_0 &= k_{vts} m_p l_p \alpha_p g. \end{aligned}$$

and

$$\frac{q_o}{q_i} = \frac{k_{vts}}{Ms^2 + m_p l_p \alpha_p g + k_{vts}} \quad (5)$$

In Figure 4 the Bode diagram of the actuating transfer function  $\frac{q_o}{\tau_i}$  is given in blue as well as  $\frac{q_o}{q_i}$  in dashed green for two stiffness values  $k_{vts} = \{75 \frac{Nm}{rad}, 400 \frac{Nm}{rad}\}$ . It becomes distinct that the natural frequency of  $\frac{q_o}{q_i}$  and the second natural frequency of  $\frac{q_o}{\tau_i}$  are highly influenced by stiffness variation, whereas the first natural frequency of  $\frac{q_o}{\tau_i}$  just slightly changes. Thus, the second natural frequency is the optimal operating point to achieve a maximum amplification of the input torque and thus, low power consumption. At this point, the phase delay between the drive position  $q_i$  and the pendulum position  $q_o$  is  $180^\circ$  and almost  $360^\circ$  for  $\frac{q_o}{\tau_i}$  which causes high control efforts.

### III. MOTION CONTROL DESIGN

For motion control of similar systems, control algorithms differing in complexity and performance are applied. For common PD-control, stability is only guaranteed, if the coordinates  $q_o$  and  $q_i$  collocate. This results in a limited controller bandwidth, which is not sufficient for operating the VTS actuator near its natural frequencies. Composite control algorithms based on singular perturbation system

TABLE I  
PARAMETERS OF MECHANICAL SETUP [11].

	Parameter	Value	Unit
VTS drive train	$k_{vts}$	56 – 475	Nm/rad
	$x_{min}$	$10.0 \cdot 10^{-3}$	m
	$x_{max}$	$155.0 \cdot 10^{-3}$	m
	$I_m$	$1.80 \cdot 10^{-4}$	kg m <sup>2</sup>
	$I_g$	$0.95 \cdot 10^{-4}$	kg m <sup>2</sup>
	$I_c$	$2.40 \cdot 10^{-3}$	kg m <sup>2</sup>
	$i_g$	80	
Pendulum	$m_p$	6.81	kg
	$M$	$9.4101 \cdot 10^{-1}$	kg m <sup>2</sup>
	$l_p$	0.46	m
	$\alpha_p$	0.7735	
	$g$	9.81	m s <sup>-2</sup>

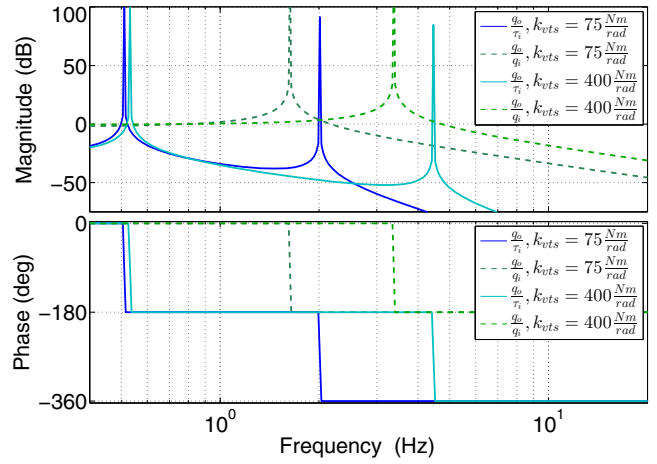


Fig. 4. Bode diagrams of transfer functions  $\frac{q_o}{\tau_i}$  and  $\frac{q_o}{q_i}$  for  $k_{vts} = \{75 \frac{Nm}{rad}, 400 \frac{Nm}{rad}\}$ .

representation require a large joint stiffness [13], which is not given in the VTS actuator. Generally suitable are rather complex nonlinear control laws like FL and PBC, which are utilized here. In addition, an extended Kalman filter as well as a simple friction compensation will be presented as parts of the control given in Figure 1.

#### A. Feedback Linearization

For the design of the FL control scheme in accordance with the block diagram in Figure 1, equations (2)-(3) are rewritten in nonlinear state space representation with the state vector

$$\mathbf{x}^T = [x_1 \ x_2 \ x_3 \ x_4]^T = [q_o \ \dot{q}_o \ q_i \ \dot{q}_i]^T. \quad (6)$$

Hence, the system is represented by

$$\begin{aligned} \dot{\mathbf{x}} &= f(\mathbf{x}) + g(\mathbf{x}) u_1, \\ \dot{\mathbf{x}} &= \begin{bmatrix} x_2 \\ -\frac{m_p g \alpha_p l_p}{M} \sin(x_1) - \frac{k_{vts}}{M} (x_1 - x_3) \\ x_4 \\ \frac{k_{vts}}{J} (x_1 - x_3) \end{bmatrix} + \begin{bmatrix} 0 \\ 0 \\ 0 \\ \frac{1}{J} \end{bmatrix} u_1, \end{aligned} \quad (7)$$

where the scalar system input  $u_1$  equals the input torque  $\tau_i$ . This torque is calculated by the scalar input transformation

$$u_1(x, z) = \frac{M J}{k_{vts}} (v(z) - a(x)), \quad (8)$$

using the nonlinear feedback term

$$\begin{aligned} a(x) &= \frac{m_p g \alpha_p l_p}{M} \sin(x_1) \left[ x_2^2 + \frac{m_p g \alpha_p l_p}{M} \cos(x_1) + \frac{k_{vts}}{M} \right] \\ &+ \frac{k_{vts}}{M} (x_1 - x_3) \left[ \frac{k_{vts}}{M} + \frac{k_{vts}}{J} + \frac{m_p g \alpha_p l_p}{M} \cos(x_1) \right] \end{aligned} \quad (9)$$

and the new input  $v(z)$  as explained in [15], [20]. Using the coordinate transformation

$$z = \begin{bmatrix} x_1 \\ x_2 \\ -\frac{m_p g \alpha_p l_p}{M} \sin(x_1) - \frac{k_{vts}}{M} (x_1 - x_3) \\ -\frac{m_p g \alpha_p l_p}{M} x_2 \cos(x_1) - \frac{k_{vts}}{M} (x_2 - x_4) \end{bmatrix}, \quad (10)$$

the components of the new state  $z$  correspond to the output position  $q_o$ , velocity  $\dot{q}_o$ , acceleration  $\ddot{q}_o$  and jerk  $\dddot{q}_o$  and the transformed system behaves like a chain of four integrators. For this system, a linear tracking control law

$$v(z) = z_d^{(4)} + k_R \tilde{z}, \quad (11)$$

aiming at asymptotic stabilization is designed. In this,  $z_d^{(4)}$  corresponds to the desired value of the fourth derivation of the transformed state  $z_1 = q_1$ ,  $\tilde{z} = z_d - z$  is the state control error and  $k_R$  are the control gains determined by placing all poles to  $s_R = -18$ .

### B. Passivity-Based Control

PBC allows a control design without cancellation of nonlinearities and achieving a good level robustness properties [21]. Through feedback control, a passivity of the closed-loop system is obtained. According to [22], this is achieved by choosing a control law such that energy is dissipated whenever  $x$  differs from the stable origin. This allows a large quantity of possible control laws. For the VTS actuator, the control algorithm proposed in [21] and applied in [23] for a FJR is implemented. The singular perturbed system description, which can be obtained of the equations (2)-(3) by eliminating  $q_i$ , is given by

$$M\ddot{q}_o = -G(q_o) + \tau_t \quad (12)$$

$$k_{vts}^{-1}\ddot{\tau}_t = -(M^{-1} + J^{-1})\tau_t + M^{-1}G(q_o) + J^{-1}\tau_i. \quad (13)$$

Equation (12) corresponds to the dynamics of a rigid robot, the control variable is however the torsional torque  $\tau_t$  and not the drive torque  $\tau_i$ . By defining a virtual *desired velocity*

$$v_o = \dot{q}_d - \Lambda(q_o - q_{o,d}), \quad (14)$$

where  $q_{o,d}$  is the desired position, a tracking error

$$s = \dot{q}_o - v_o \quad (15)$$

is obtained. Note that this tracking error depends on the velocity error and a position error weighted by  $\Lambda$ . The control algorithm proposed for subsystem (13) is

$$\tau_d = M\dot{v}_o + G(q_o) - k_s s, \quad (16)$$

where  $\tau_d$  is the desired joint torque and

$$\tau_i = (1 + JM^{-1})\tau_t - JM^{-1}G(q_o) + J(k_{vts}^{-1}\ddot{\tau}_d + k_d\dot{e}_\tau + k_p e_\tau), \quad (17)$$

for torque dynamics control, with torque error  $e_\tau = \tau_d - \tau_t$ . A drawback of PBC is that there is no straightforward way to tune the gains  $k_p$ ,  $k_d$ ,  $\Lambda$  and  $k_s$  hence these are selected heuristically based on experimental results as given in Table II. Besides, the coordinate  $q_o$  up to the fourth derivative must be measured, estimated or computed from  $x$  in analogy with (10).

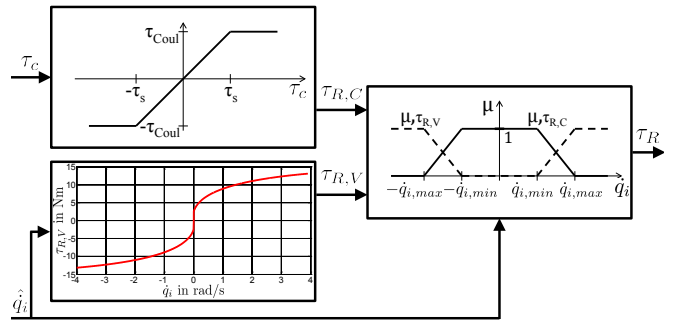


Fig. 5. Principle of friction compensation modified from [25].

### C. Friction Compensation

Due to the occurrence of gearbox friction, control performance can be increased by compensating such effects. For this purpose, friction parameters are identified experimentally and approximated via a nonlinear least squares regression using a friction model presented in [24]:

$$\tau_R(\dot{q}_i) = \underbrace{\text{sgn}(\dot{q}_i)\tau_{Coul}}_{\text{Coulomb}} + \underbrace{\sigma\dot{q}_i}_{\text{Viscous}} + \underbrace{\text{sgn}(\dot{q}_i)(\tau_{Stri} - \tau_{Coul})\exp\left(-\left|\frac{\dot{q}_i}{V_S}\right|^\delta\right)}_{\text{Stribeck}}. \quad (18)$$

The model consists of a Coulomb and viscous part plus a part to shape the Stribeck effect in the low-velocity Stribeck region. Experimentally identified parameters are given in Table II. The second block in Figure 5 shows the regression with the torque increasing continuously from the static friction level of  $\tau_{Coul} = 2.4025 \text{ Nm}$ , which is achieved by a negative shape factor  $\delta = -0.1309$ . Figure 5 depicts the compensation scheme composed of a velocity dependent part generating  $\tau_{R,V}$ , a part  $\tau_{R,C}$  depending on the linear control and a third part composing the output  $\tau_R$  by a weighted sum of the previous parts depending on the actuator velocity [25].

### D. Extended Kalman Filter

The differentiation of the position signal led to a noisy velocity signal, which could not be smoothed sufficiently by low pass filtering without a phase delay. Hence, an EKF is used to estimate  $\hat{x} = [\hat{q}_o \ \dot{\hat{q}}_o \ \hat{q}_i \ \dot{\hat{q}}_i]$  from the position signals  $q_o$ ,  $q_i$  and the controller output  $\tau_c$ . The EKF theory and its application is presented in [26]. The jacobian of the system matrix  $f(x)$  of the state space representation (7) is

$$\mathbf{A}_k = \begin{bmatrix} 0 & 1 & 0 & 0 \\ -\frac{m_p l_p \alpha_p g \cos(q_o)}{M} - \frac{k_{vts}}{M} & 0 & \frac{k_{vts}}{M} & 0 \\ 0 & 0 & 0 & 1 \\ \frac{k_{vts}}{J} & 0 & -\frac{k_{vts}}{J} & 0 \end{bmatrix}, \quad (19)$$

and the measurement matrix

$$\mathbf{H}_k = \begin{bmatrix} 1 & 0 & 0 & 0 \\ 0 & 0 & 1 & 0 \end{bmatrix}. \quad (20)$$

The parameters of the covariance matrices of the process noise  $\mathbf{Q}$  and measurement noise  $\mathbf{R}$  are defined heuristically and shown in Table II. Since the influence of noise on system states and measurement is unknown, the matrices are set to be  $\mathbf{V}_k = 1$  and  $\mathbf{W}_k = 1$  respectively.

#### IV. EXPERIMENTAL EVALUATION

For the experiments, a cRIO realtime system from NI Germany GmbH, Munich is used to implement the controllers running at a sampling frequency of  $f_s = 1k Hz$ . The control methods are analyzed in terms of accuracy, dynamics and their energy consumption based on a sinusoid with frequency of  $2 Hz$  and an amplitude of  $0.0873 rad$  and a sigmoidal step reaching an amplitude of  $0.1745 rad$  after  $0.6 s$ . For motion planning, polynomial trajectories are developed according to [27]. The drive train stiffness is set to  $k_{vts} = 75 \frac{Nm}{rad}$ , which results in maximum amplification of the input torque in case of the sinusoid according to Figure 4. With the sinusoid the focus is set on the analysis of dynamics and energy consumption, whereas accuracy is evaluated by the step response.

In Figure 6 the system response to a sigmoidal step and the corresponding input torque is shown applying FL and PBC. Both controllers do not reach the exact final value and FL overshoots. After  $3 s$ , the static error is  $q_{o,d} - q_o = -0.008 rad$  on the pendulum side, whereas the deviation on the drive side is  $q_{i,d} - q_i = -0.0012 rad$ . The difference between the deviations indicates that the model parameters are slightly inaccurate. The final position of PBC is  $q_{o,d} - q_o = 0.0226 rad$  lower than the desired position thus, the deviation is greater in magnitude compared to the FL result. Input torque curves of both controllers are qualitatively similar. However, PBC shows a high sensitivity to position steps of coordinate  $q_o$  whereas the output torque of FL is smoother and reaches higher values. Taking this into account,

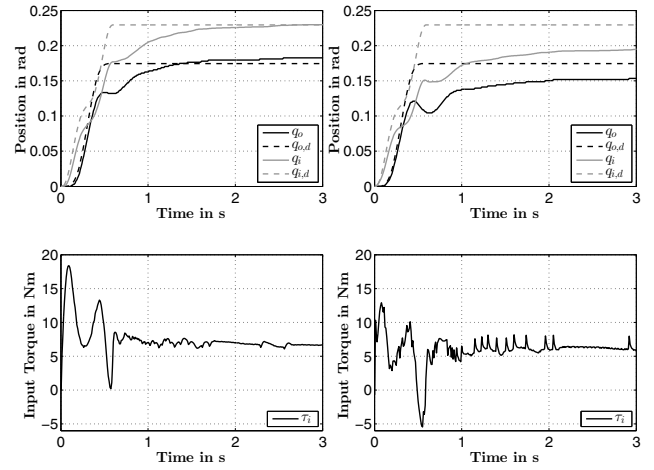


Fig. 6. Position and input torque response to a sigmoidal trajectory applying the FL (left) and PBC (right).

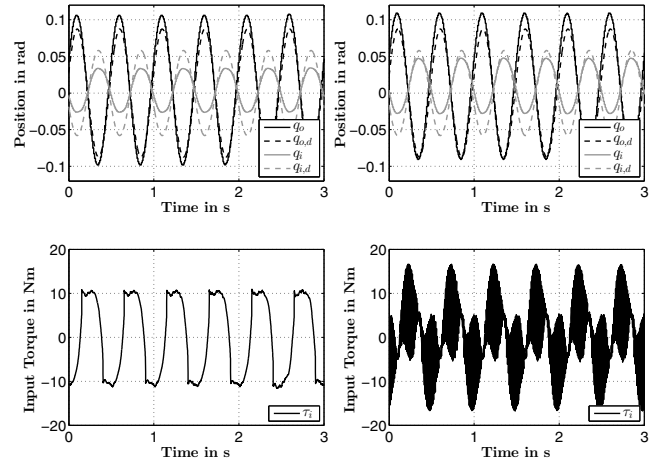


Fig. 7. Position and input torque response to a sinus trajectory (Frequency of  $2 Hz$  and an amplitude of  $0.0873 rad$ ) applying the FL (left) and PBC (right).

TABLE II

PARAMETERS OF CONTROLS, FILTERS AND FRICTION COMPENSATION.

	Parameter	Value	Unit
Control	$s_R$	$[-10 - 10 - 10 - 10]$	
	$k_p$	100	
	$k_v$	20	$s$
	$k_d$	10	$kg \cdot \frac{m}{s}$
	$\Lambda$	10	$s^{-1}$
EKF	$\mathbf{Q}$	$diag(10^{-3} \ 10^{-1} \ 10^{-3} \ 10^{-1})$	
	$\mathbf{R}$	$diag(10^{-1} \ 10^{-1})$	
Friction Compensation	$\tau_s$	0.005	$Nm$
	$\tau_{Coul}$	2.4025	$Nm$
	$\tau_{Stri}$	376.0605	$Nm$
	$\delta$	-0.1309	
	$\sigma$	-0.8038	$Ns$
	$V_S$	$3.5570e^4$	
	$\dot{q}_{i,max}$	$7 \cdot 10^{-3}$	$\frac{rad}{s}$
	$\dot{q}_{i,min}$	$5 \cdot 10^{-3}$	$\frac{rad}{s}$

it is difficult to evaluate the accuracy of PBC.

Figure 7 shows the system behavior if a sinus trajectory is applied. Both controllers lead to a stable oscillation with sufficiently high dynamics and a slight superelevation. With same stiffness and higher frequencies the amplitude tends to result in an increase of the superelevation and with lower frequencies this dynamic effect inverts. Since the system is operated in the second natural frequency and hence beyond the antiresonance the phase delay between  $q_i$  and  $q_o$  is  $180^\circ$  which corresponds to the system analysis in Section II-C. As in the case of the step, the output torque of the PBC is superposed with chattering which is due to the discrete sensor signal whereas the FL output is smooth. This circumstance doesn't allow a fair comparison of energy consumption. Control effort increases with the oscillation frequency, as dynamic requirements are rising. Figure 8 shows that stable control can be reached at a frequency of  $3,2 Hz$  and stiffness set to  $k_{vts} = 200 \frac{Nm}{rad}$  enabling exploitation of the second natural frequency.

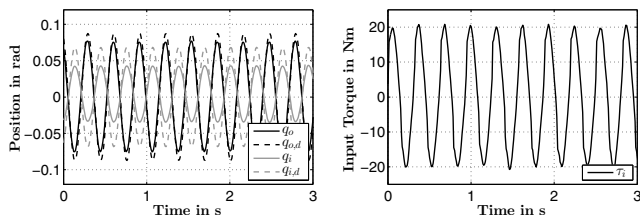


Fig. 8. Position and input torque response to a sinus trajectory (Frequency of 3, 2 Hz and an amplitude of 0.0873 rad) applying FL.

## V. CONCLUSIONS

In this paper experimental results comparing FL and PBC for motion control of an prototypical actuator with variable torsion stiffness are shown. Based on the mechanical model of the experimental setup that is given in Section II, the control designs are described in Section III together with a friction compensation and an extended Kalman filter. Both controllers are analysed considering criteria assessing stability, dynamics, accuracy and commanded torque. Using sinusoidal trajectories, it is shown that PBC and FL lead to stable control with high dynamics though both controllers lack in robustness due to the model-based approach. However, examining a sigmoidal trajectory shows that a larger steady-state deviation is caused by PBC. This is due to the high sensitivity to the discrete position signal which results in a noisy input torque  $\tau_i$ . Overall, with FL better results are obtained. By increasing the stiffness and the oscillation frequency, it is further shown that FL is suitable, if stiffness is adapted to the systems movement and hence subject for future research. Such will include further improvement of VTS controls in terms of the mentioned assessment criteria and the automation of stiffness adjustment. Thereupon, experiments with continuously varying stiffness during pendulum motion can be realized and benefits of VTS during dynamic operation, which finally might support prosthetics or other wearable robotics, can be clarified.

## ACKNOWLEDGMENT

The authors thank Bühler Motor GmbH and National Instruments Germany for hardware donations.

## REFERENCES

- [1] R. Van Ham, T. G. Sugar, B. Vanderborght, K. W. Hollander, and D. Lefeber, "Compliant Actuator Designs Review of Actuators with Passive Adjustable Compliance/Controllable Stiffness for Robotic Applications," *IEEE Robotics & Automation Magazine*, vol. 16, pp. 81–94, 2009.
- [2] G. A. Pratt and M. M. Williamson, "Series elastic actuators," in *Proceedings of the 1995 IEEE/RSJ International Conference on Intelligent Robots and Systems*, 1995.
- [3] S. Klug, T. Lens, O. von Stryk, B. Möhl, and A. Karguth, "Biologically inspired robot manipulator for new applications in automation engineering," in *Proc. of Robotik 2008*, 2008.
- [4] B. Vanderborght, R. Van Ham, D. Lefeber, T. G. Sugar, and K. W. Hollander, "Comparison of Mechanical Design and Energy Consumption of Adaptable, Passive-compliant Actuators," *The International Journal of Robotics Research*, vol. 28, pp. 90–103, 2009.
- [5] M. M. Williamson, "Series elastic actuators," Master Thesis, Massachusetts Institute of Technology, 1995.

- [6] T. Morita and S. Sugano, "Design and development of a new robot joint using a mechanical impedance adjuster," in *1995 IEEE International Conference on Robotics and Automation*, 1995.
- [7] B. Vanderborght, A. Albu-Schaeffer, A. Bicchi, E. Burdet, D. G. Caldwell, R. Carloni, M. Catalano, O. Eiberger, W. Friedl, G. Ganesh, M. Garabini, M. Grebenstein, G. Grioli, S. Haddadin, H. Hoppner, A. Jafari, M. Laffranchi, D. Lefeber, F. Petit, S. Stramigioli, N. Tsagarakis, M. Van Damme, R. Van Ham, L. C. Visser, and S. Wolf, "Variable impedance actuators: A review (2013)," *Robotics and Autonomous Systems*, 2013.
- [8] K. W. Hollander, R. Ilg, T. G. Sugar, and D. Herring, "An efficient robotic tendon for gait assistance," *Journal of Biomechanical Engineering*, vol. 128, pp. 788 – 791, 2006.
- [9] J. W. Hurst, J. E. Chestnutt, and A. A. Rizzi, "An actuator with physically variable stiffness for highly dynamic legged locomotion," in *2004 IEEE International Conference on Robotics and Automation*, 2004.
- [10] B. Vanderborght, N. G. Tsagarakis, R. Ham, I. Thorson, and D. G. Caldwell, "MACCEPA 2.0: compliant actuator used for energy efficient hopping robot Chobino1D," *Autonomous Robots*, vol. 31, pp. 55–65, 2011.
- [11] J. Schuy, P. Beckerle, J. Wojtusich, S. Rinderknecht, and O. von Stryk, "Conception and Evaluation of a Novel Variable Torsion Stiffness for Biomechanical Applications," in *IEEE International Conference on Biomedical Robotics and Biomechatronics*, 2012.
- [12] P. Tomei, "A simple PD controller for robots with elastic joints," *IEEE Transactions on Automatic Control*, vol. 36, no. 10, pp. 1208–1213, 1991.
- [13] M. Spong, J. Y. Hung, S. Bortoff, and F. Ghorbel, "A comparison of feedback linearization and singular perturbation techniques for the control of flexible joint robots," in *American Control Conference, 1989*, 1989, pp. 25–30.
- [14] C. Ott, C. Ott, A. Kugi, and G. Hirzinger, "On the passivity-based impedance control of flexible joint robots," *IEEE Transactions on Robotics*, vol. 24, no. 2, pp. 416–429, 2008.
- [15] A. W. Spong, "Modeling and control of elastic joint robots," *Journal of Dynamic Systems, Measurement, and Control*, vol. 109, pp. 310–318, 1987.
- [16] C. Ott, A. Albu-Schaeffer, A. Kugi, S. Stamigioli, and G. Hirzinger, "A passivity based cartesian impedance controller for flexible joint robots - part i: torque feedback and gravity compensation," in *2004 IEEE International Conference on Robotics and Automation, 2004. Proceedings. ICRA '04*, vol. 3, 2004, pp. 2659–2665 Vol.3.
- [17] G. Palli and C. Melchiorri, "Robust control of robots with variable joint stiffness," in *Advanced Robotics, 2009. ICAR 2009. International Conference on*, 2009, pp. 1–6.
- [18] P. Beckerle, J. Wojtusich, J. Schuy, B. Strah, S. Rinderknecht, and O. Stryk, "Power-optimized stiffness and nonlinear position control of an actuator with variable torsion stiffness," in *2013 IEEE/ASME International Conference on Advanced Intelligent Mechatronics (AIM)*, 2013, pp. 387–392.
- [19] D. Gross, W. Hauger, J. Schröder, and W. A. Wall, *Technische Mechanik 3: Kinetik*. Springer, 2010.
- [20] J.-J. E. Slotine and W. Li, *Applied Nonlinear Control*. Prentice hall International Inc., 1991.
- [21] B. Brogliato, R. Ortega, and R. Lozano, "Global tracking controllers for flexible-joint manipulators: a comparative study," *Automatica*, vol. 31, no. 7, p. 941–956, 1995.
- [22] H. K. Khalil, *Nonlinear systems*. Upper Saddle River, N.J.: Prentice Hall, 2002.
- [23] A. Albu-Schaeffer, "Regelung von Robotern mit elastischen Gelenken am Beispiel der DLR-Leichtbauarme," Dissertation, Technische Universität München, München, Sep. 2001.
- [24] M. Ruderman, "Zur Modellierung und Kompensation dynamischer Reibung in Aktuatorssystemen," Dissertation, Technische Universität Dortmund, Dortmund, Aug. 2012.
- [25] S. Rinderknecht and B. Strah, "Simple and effective friction compensation on wheeled inverted pendulum systems," in *MEDYNA 2013 - 1st Euro-Mediterranean Conference on Structural Mechanics and Vibroacoustics*, Marrakech, Marokko, Apr. 2013.
- [26] G. Welch and G. Bishop, "An introduction to the kalman filter," University of North Carolina at Chapel Hill, Chapel Hill, NC, USA, Tech. Rep., 1995.
- [27] B. Siciliano, L. Sciavicco, L. Villani, and G. Oriolo, *Robotics: Modelling, Planning and Control*, 1st ed. Springer, Dec. 2008.